Journal of Magnetism and Magnetic Materials 513 (2020) 166993

Contents lists available at ScienceDirect

Journal of Magnetism and Magnetic Materials

journal homepage: www.elsevier.com/locate/jmmm

Research articles

Dipolar interactions among magnetic dipoles of iron oxide particles dispersed in mili-size hydrogel beads

D.G. Actis[a], G.A. Muñoz Medina[a], A.A. Velásquez[b], C. Pereda[c], L.M. Sanchez[c], V.A. Alvarez[c], D. Muñetón Arboleda[d], P. Mendoza Zélis[a,*], F.H. Sánchez[a,*]

[a] Instituto de Física La Plata, CONICET – Universidad Nacional de La Plata, Casilla de Correos 67, La Plata, Argentina
[b] Grupo de Electromagnetismo Aplicado, Universidad EAFIT, A.A. 3300, Medellín, Colombia
[c] Materiales Compuestos Termoplásticos, Instituto de Investigaciones en Ciencia y Tecnología de Materiales, CONICET – Universidad Nacional de Mar del Plata, Mar del Plata, Argentina
[d] Centro de Investigaciones Ópticas (CIOp) (CONICET La Plata-CIC-UNLP), Gonnet, La Plata, Buenos Aires, Argentina

A B S T R A C T

The recently published Mean Field Interacting Superparamagnet Model (MFISP model), which introduces the effective demagnetizing factor N^E, is tested in specimens having a random-like spatial distribution of magnetic nanoparticles, where different hierarchies of clustering are present. These specimens are ferrogel PVA/iron oxide beads synthesized by a one-pot route, having spheroidal shapes and sizes of about 1 mm, and chain and disk-like arrays (superstructures) of beads. Raman analyses indicated that magnetic nanoparticles are composed by a mixture of magnetite and maghemite. Beads swell 208% by hydration in about 40 min.

The increase of the ac susceptibility as a function of hydration time closely reflects the effect of bead swelling, in agreement with the expected diminution of dipole–dipole interactions. Measured susceptibility is analyzed in terms of the susceptibility χ of non-interacting particles and the effective demagnetizing factor N^E of the specimen, which depends on swelling. The Specific Absorption Rate of electromagnetic power by the beads grows with the hydration time in agreement with ac susceptibility behavior.

For long hydration times susceptibility and high field magnetization decrease. This is explained by the occurrence of oxidation of magnetite/maghemite to hematite.

Isothermal magnetization experiments are performed on each superstructure in two perpendicular principal directions each. Results are consistently described with the MFISP model by considering two hierarchies of clustering: beads themselves and clusters within the beads.

From the whole set of experiments, it is possible to estimate values for the volume fractions of particles in clusters and clusters in beads, given by $x_{pc} = 0.46(15)$ and $x_{cb} = 0.16(5)$. The susceptibility of non-interacting particles, $\chi = 13(4)$, is also obtained, which results about five times larger than the measured (apparent) one.

The MFISP model proves to be a convenient and efficient tool for the analysis of magnetization studies of complex 3d dispersions of magnetic nanoparticles, allowing an experimental determination of relevant physical information, otherwise not accessible by magnetic measurements.

1. Introduction

For several applications, magnetic nanoparticles (referred to hereafter as “particles”) are suspended, stored and handed in the form of stable colloids, which are magnetically characterized in this state. However, for a given application, particles are administrated into a target where their magnetic response may differ considerably, among other reasons, because the target imposes a specific spatial distribution, and consequently, interparticle interactions with different intensities and geometries appear [1,2]. For some applications particles are incorporated into, or synthesized inside hydrogels creating in this way magnetic hydrogels which are commonly named ferrogels (FGs from here on). For biomedical or remediation purposes FGs can be either transitorily loaded with beneficial substances [3] and be later remotely actuated to deliver them accurately on demand [4], or be used as contaminants getters in order to remove them from the environment [5]. Since particles’ distribution inside FGs is usually complex and unknown *a priori*, it is of crucial importance to gain reliable knowledge on the physics of how particles respond to magnetic stimuli when they are included in these materials in comparison to their intrinsic response, i.e. when they do not interact with each other.

FGs are soft versatile materials with unique properties. A FG is an interconnected micrometer-scale porous structure of crosslinked polymer chains with the particles attached to it, and can swell several times its dry volume by absorption of water. Additionally, FGs can be tailored in the form of biocompatible micro- and nano-beads, which can be directed to, and localized at, target places where the substance delivery is needed [6].

* Corresponding authors.
E-mail addresses: pmendoza@fisica.unlp.edu.ar (P. Mendoza Zélis), sanchez@fisica.unlp.edu.ar (F.H. Sánchez).

https://doi.org/10.1016/j.jmmm.2020.166993
Received 13 February 2020; Received in revised form 21 April 2020; Accepted 10 May 2020
Available online 23 May 2020
0304-8853/

It is necessary to have a simple and reliable model, based on experimental evidence, to estimate the dependence of the interactions on the main parameters of the particles' distribution. This distribution can be described allowing for different levels of clustering, taking into consideration characteristic distances, as interparticle and intercluster ones, and the shapes of clusters and sample (or superstructure). Polyvinyl alcohol (PVA)/iron oxide FGs with random-like distribution of particles are almost ideal benchmarks to this end. In particular, their hydration produces almost isotropic swelling, increasing several times its initial volume and interparticle separations. Therefore, it is necessary to study the influence of the spatial arrangement of particles in clusters, clusters in beads and, eventually, beads in superstructures. For example, FG milli-beads, similar in composition, shape and size, can be purposely arranged into different superstructures in order to observe the effect of the array geometry on their magnetic response.

In this paper, millimetric-size, PVA/Fe oxide FG beads were synthesized through a one pot route. FG swelling by hydration was used to modify the intensity of dipole–dipole interactions, due to the enlargement of interparticle mean distance. Furthermore, beads were arranged into chain and disk-like arrays to observe the effect of superstructure and its dependence on the excitation-measurement direction. The magnetic response of these particles' ensembles was recorded by VSM magnetometry, ac susceptibility, and specific absorption rate (SAR) of energy from radiofrequency irradiation. The mean field interacting superparamagnet (MFISP) model, which evaluates the effect of dipolar interactions by defining an effective demagnetizing tensor [7,8] was used to analyze the results. These demonstrate that density and geometry of the particles' distribution affects the magnetic susceptibility of the ensembles consistently with the theoretical expectations of the model. We hope that this study will help to understand the magnetic response of ferrogel beads under specific conditions, alone, in simple arrays, either dry or hydrated, and will be useful for the design of magnetically driven remote applications.

2. Materials and methods

2.1. Materials

Polyvinyl alcohol was supplied by Sigma-Aldrich (Molecular weight 89000–98000 g/mol, hydrolysis degree of 98–99%). For iron oxides preparation, two different iron salts were used as precursor materials for cations Fe^{2+} and Fe^{3+}: $FeSO_4{\cdot}7H_2O$ and $FeCl_3{\cdot}6H_2O$, respectively (both from Cicarelli Laboratory, Argentina). Other reactants were also incorporated to produce the alkaline hydrolysis of iron cations: NaOH (Biopack, Argentina) and bidistilled water.

2.2. Methods

2.2.1. Magnetic PVA beads preparation

An aqueous Polyvinyl alcohol solution (5 w/v %) was prepared under constant stirring at 85 °C. Then, $FeSO_4{\cdot}7H_2O$ (0.612 g) and $FeCl_3{\cdot}6H_2O$ (1.186 g) salts were added, and the stirring and heating were kept constant for 30 min. After this, the solution was cooled to room temperature to be dropped onto a NaOH solution, where the magnetic beads were almost instantaneously formed. Once again, the stirring was kept constant for 30 min and then the beads were washed with distilled water. The samples were then frozen (−18 °C, 1 h) and after that they were placed at room temperature (25 °C, 1 h), completing 3 of these freezing-thawing (F-T) cycles, and thus obtaining physically cross-linked hydrogels through the F-T method [9]. The prepared beads were finally dried at 40 °C.

2.2.2. Techniques

Scanning Electron Micrographs (SEM) were obtained in a JEOL JSM-6460 LV instrument. Samples have been previously swollen, frozen, lyophilized, cryofractured with N_2 liquid and sputtered with gold.

Thermogravimetric Analysis (TGA) was conducted in a TA-Q500 equipment from room temperature to 900 °C at a heating rate of 10 °C/min under both air and N_2 atmospheres in order to determine the mass ratio of magnetic particles in the beads.

Isothermal magnetization cycles were obtained with a LakeShore 7104 Vibrating Sample Magnetometer (VSM), varying the applied field H^A in the interval $19000\ \text{Oe} \leq H^A \leq 19000\ \text{Oe}$ at 82 Hz. Measurements were carried out on single beads with typical masses between 1.1 and 1.4 mg, and on arrays of three or seven beads as described below.

Ac magnetic susceptibility was measured on dry and hydrated beads at room temperature (RT), at several excitation frequencies f from 8 to 8200 Hz and under applied fields amplitudes H_0^A of 1 and 10 Oe. The dependency of ac susceptibility on hydration/swelling time was recorded on one bead at f= 825 Hz and H_0^A= 1 Oe, during more than three days.

Determinations of Specific Absorption Rate (SAR) of electromagnetic power were performed on one sample of four beads at different hydration times with a Hüttinger 2.5/3.0 generator using a 25 mm inner-diameter duty-coil at 22 °C.

Micro-Raman spectra were acquired with a Horiba-Jobin Yvon XPlora Plus confocal scanning microscope. For these measurements, a dry and a hydrated beads were placed on a glass cover slide. Raman spectra were recorded at room temperature in different zones of the sample with a 100 × objective (laser spot diameter of 2 μm) and laser power less than 0.8 mW, low enough to avoid sample damage and/or denaturalization.

3. Results and discussion

3.1. Beads morphology and chemical characterization

SEM micrographs of the beads surface indicate that the prepared materials have a highly porous morphology with well-defined pores having a hierarchical structure, (see Fig. 1).

The chemical phases of the particles present in the beads were analyzed by confocal Raman spectroscopy. It was found that particles of virgin beads (never hydrated after preparation) can be described as a mixture of magnetite and maghemite (see Section 3.3.3).

3.2. Beads hydration and swelling.

Fig. 2 shows beads of FG on a Vernier scale. They have mean diameters of the order of 1 mm. Taking several pictures of the one bead from different angles, and using an *ad hoc* Matlab code to count the bead pixels, the mean area A was measured. Volume was then calculated as $V = \frac{4}{3}\pi^{-1/2}A^{3/2}$. From bead volume V_b and mass m_b, measured with a precision scale (to the hundredth of mg), the corresponding density was obtained as $\rho_b = \frac{m_b}{V_b} = 1.4(1)\ \text{g/cm}^3$. From TGA experiments, the mass fraction of magnetic particles in the ferrogel was

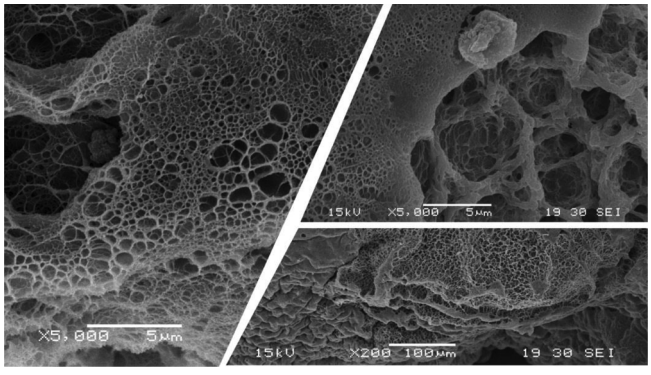

Fig. 1. SEM micrographs of ferrogel beads.

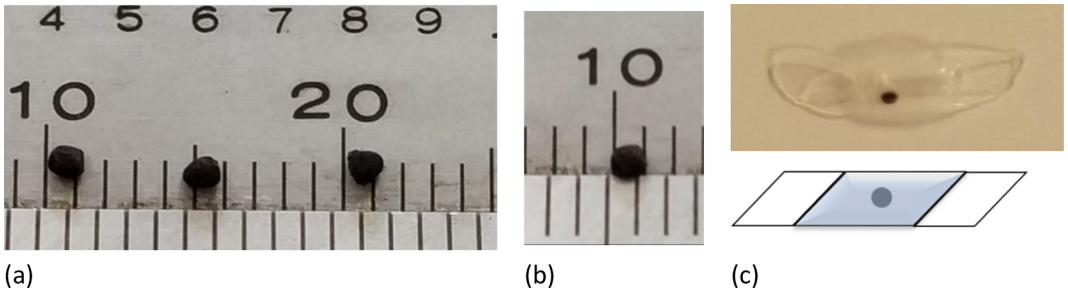

Fig. 2. (a) FG beads on a Vernier scale. (b) Bead with a mean diameter of 1.17(12) mm. (c); up: photo of bead encapsulated with water in a thermo-shrinkable tube; down: scheme showing the central part with bead in water and the sealed ends of the tube.

estimated as $x_{pb}^{m} = 0.26(1)$. By combining size and gravimetry measurements, and assuming a density $\rho_{mag} = 5.0(1)$ g/cm^3 for the magnetic particles (average between magnetite and maghemite values), a volume fraction of iron oxide particles in the beads, $x_{pb} = (\rho_b/\rho_{mag})x_{pb}^{m} = 0.073(6)$, was determined.

Hydration of beads was carried out by immersion into milliQ water. Swelling, relative to the initial dry volume, was observed by taking photographs every 10 s. Area A_b of a bead major section was obtained by counting the pixels of the bead image using an *ad hoc* matlab code, and volume was calculated as $V_b = \frac{4}{3}\pi^{-1/2}{A_b}^{3/2}$. Relative percent values of A_b and V_b were obtained as $A_{br}(t) = 100(A_b(t) - A_{b0})/A_{b0}$ and $V_{br}(t) = 100(V_b(t) - V_{b0})/V_{b0}$, where A_{b0} and V_{b0} are the section-area and volume values at $t = 0$, i.e., when hydration begins. Fig. 3 shows an example of relative area and volume swelling curves. It is observed that beads swell up to about 200% their initial volumes. Assuming isotropic and uniform swelling, separation between two points fixed to the bead, experience a maximum increase of approximately 44%. Swelling measured photographically agrees, within experimental error, with conventional gravimetric determinations.

3.3. Dependency of magnetic properties and composition on swelling and hydration time

3.3.1. Low field ac susceptibility

The susceptibility of one dry bead was measured at room temperature (RT) for several frequencies, as shown in Fig. 4(a). It was immediately encapsulated along with 50 μL of milliQ water in a clear thermo-shrinkable tube (see Fig. 2(c)) and then its susceptibility was recorded at 825 Hz as a function of time (Fig. 4(b)). First recording data was obtained 10.23 min after immersion in water. Measurement was carried on during 1.86 days. Data indicated by a red star, is an average of values recorded on the dry bead, before hydration, at several field frequencies between 8 and 10^4 Hz and amplitudes of 1 and 10 Oe. Grey bar on the right indicates the average value recorded on the hydrated bead, at the same frequencies and amplitudes, one day after measurement as a function of time was finished (average of data indicated by blue and magenta triangles in Fig. 4a).

It is observed that susceptibility increases rapidly during the first 34 min, continues increasing at a slower pace up to about 580 min, and finally decreases up to the end of the experiment, suggesting that there is a tendency to saturate. In Fig. 4(c) we present a comparison of appropriately normalized values of bead volume and susceptibility as a function of time, for the first 180 min. It can be observed, that both curves closely follow each other during the first 40 min, approximately, indicating an almost linear correlation between both quantities. Indeed, a susceptibility increase is expected to occur during swelling, since dipole–dipole interactions diminish due to the increasing separation between particles. In a random 3d distribution of particles, interactions give rise to a demagnetizing field $\vec{H}^{D}$ which may be approximated by

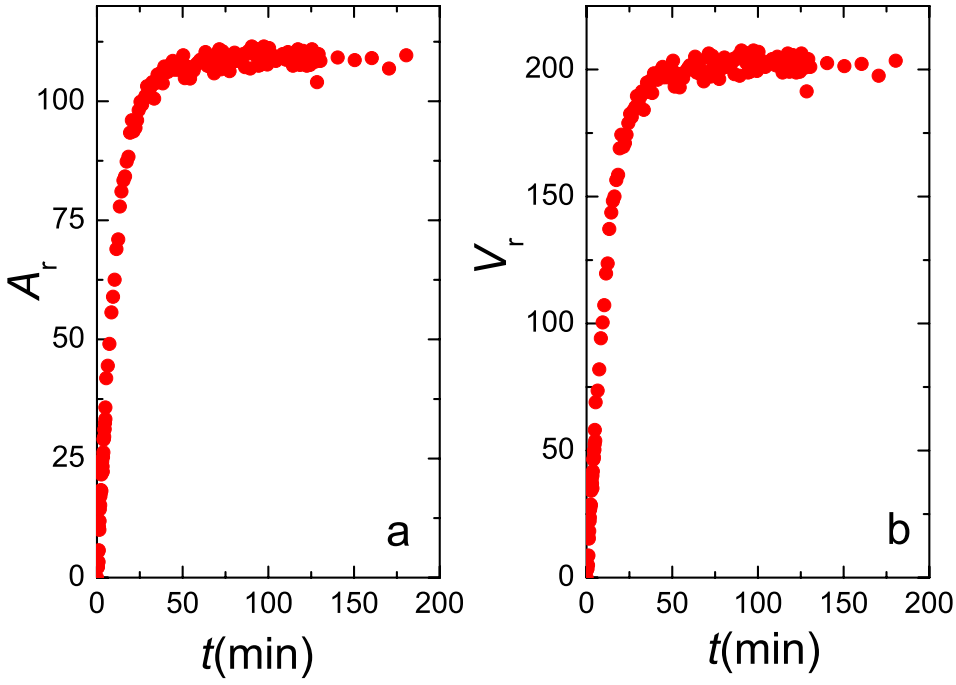

Fig. 3. (a) Relative area A_{br} and (b) relative volume V_{br} swelling as a function of hydration time.

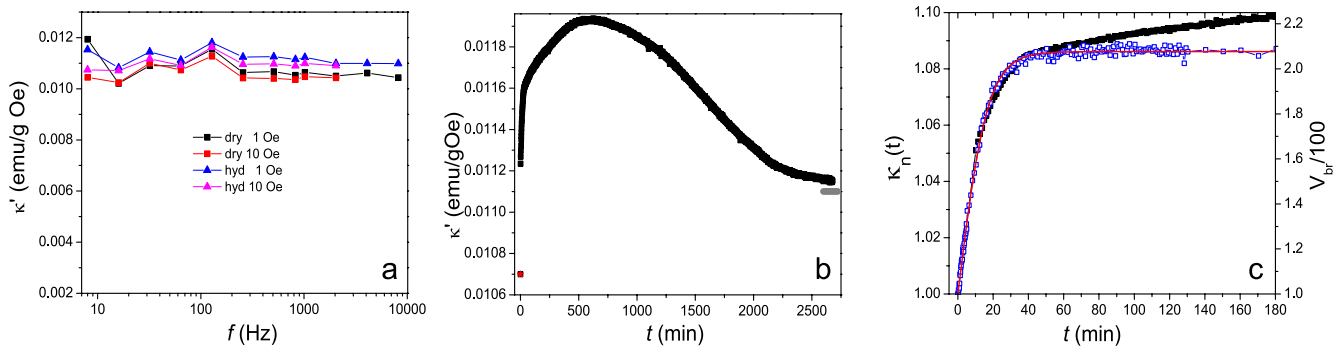

Fig. 4. (a) susceptibility of the dry and hydrated bead for several applied field frequencies, using ac field amplitudes of 1 and 10 Oe. (b) Susceptibility of the same bead as a function of hydration time at 825 Hz using a field amplitude of 1 Oe. (c) Comparison of normalized values of volume and susceptibility (at 825 Hz) as a function of time, for the first 180 min of hydration. Red line is the fit of the swelling data with function $f_b(t) = V_b(t)/V_{b0} = f_b^{inf} + 2(1 - f_b^{inf})/(1 + e^{t/\tau_b})$, where $V_b(t)$ is the bead volume at time t and V_{b0} its initial value (see text). (For interpretation of the references to colour in this figure legend, the reader is referred to the web version of this article.)

$\vec{H}^D = -N^E\vec{M}$, where M is the magnetization and N^E is the principal component of an effective demagnetizing tensor in the measurement direction [10]. Under these circumstances the effective field $\vec{H}^E = \vec{H}^A + \vec{H}^D$, where H^A is the amplitude of the applied field, has a smaller intensity than H^A, leading to a reduced apparent susceptibility

$$\kappa = \frac{\chi}{(1 + N^E\chi)}, \tag{1}$$

where χ is the *real* susceptibility, i.e., the susceptibility in the absence of interactions. Therefore, we expect a diminution of N^E on swelling, and a consequent augment of κ. A simplified expression for N^E, equivalent to the one given in [7] is

$$N^E = x_{pb}(N^b - N^c) + x_{pc}N^c \tag{2}$$

It allows for the particles to be aggregated in clusters and it assumes that field is applied, and measurement is made, along one principal direction. x_{pc} and x_{cb} are the volume fractions of particles in clusters and clusters in the bead, respectively, being $x_{pb} = x_{pc}x_{cb}$ the volume fraction of particles in the bead. N^c and N^b are the magnetostatic demagnetizing factors [10] corresponding to clusters and bead shapes. N^c must be taken as an average over the bead.

We define the swelling factor of the bead as $f_b(t) = V_b(t)/V_{b0}$ (experimental bead swelling is represented in Fig. 4(c) by blue squares), and the swelling factor of the clusters as $f_c(t) = V_c(t)/V_{c0}$. The volume fractions introduced in (2) can be expressed in terms of these factors

$$x_{pb}(t) = \frac{n_{cb}n_{pc}V_p}{V_b(t)} = \frac{n_{cb}n_{pc}V_p}{V_{b0}f_b(t)} = \frac{x_{pb0}}{f_b(t)},$$

$$x_{pc}(t) = \frac{n_{pc}V_p}{V_c(t)} = \frac{n_{pc}V_p}{V_{c0}f_c(t)} = \frac{x_{pc0}}{f_c(t)} \tag{3}$$

We have observed that swelling proceeds isotropically, therefore we will assume that N^b and N^c do not vary with time. Consequently, N^E can be expressed as

$$N^E(t) = \frac{x_{pb0}}{f_b(t)}(N^b - N^c) + \frac{x_{pc0}}{f_c(t)}N^c \tag{4}$$

$f_b(t)$ was obtained from fitting the swelling $V_b(t)$ data with the function

$$f_b(t) = f_b^{inf} + \frac{2(1 - f_b^{inf})}{\left(1 + e^{\frac{t}{\tau_b}}\right)}, \tag{5}$$

with $f_b^{inf} = 2.077(1)$, $\tau_b = 8.4(1)$ min (see red line in Fig. 4(c)), and $x_{pb0} = x_{pc0}x_{cb0}$ matching the experimental value $x_{pb0} = 0.073(6)$. Finally, we will take into account the specific configurations of specimen and experiment. Beads are spheroids, then $N^b = 1/3$. On the other hand, since clusters are expected to be oriented randomly, the average cluster demagnetizing factor should also be $N^c = 1/3$. In the case of the hydration experiments, the bead is encapsulated with water, having some motion freedom which further randomizes bead and clusters geometry. Therefore, it is a very good approximation to assume that $N^b = N^c = 1/3$. Hence, $N^E(t)$ becomes

$$N^E(t) = \frac{x_{pc0}}{3f_c(t)}, \tag{6}$$

where x_{pc0} and $f_c(t)$ are unknown. To proceed further, we will analyze the experimental evolution of $\kappa(t)$ in the interval of time from 0 to 180 min, which adds χ as a new unknown (see Eq.(1)). Notice that $x_{pc0} \geq x_{pb0}$. In fact, if particles were closely packed in clusters, $x_{pc0} = 1$. We have chosen to work with the apparent susceptibility κ_n normalized at $t = 0$ min (Fig. 4(c)), which is related to χ by

$$\kappa_n(t) = \frac{1 + N^E(0)\chi}{1 + N^E(t)\chi} = \frac{1 + x_{pc0}\chi/3}{1 + x_{pc0}\chi/3f_c(t)}, \tag{7}$$

For the fitting process we will consider $y_{pc} = x_{pc0}\chi$ as a single parameter, and propose for $f_c(t)$ a function alike to $f_s(t)$, plus an additional term to take into account the growth of κ_n observed at times beyond 40 min,

$$f_c(t) = f_c^{inf} + \frac{2(1 - f_c^{inf})}{\left(1 + e^{\frac{t}{\tau_c}}\right)} + ct \tag{8}$$

Therefore, the set of fitting parameters is y_{pc}, f_c^{inf}, τ_c and c. Best fit is shown in Fig. 5 and corresponds to $y_{pc} = 5.8(2)$, $f_c^{inf} = 1.130(1)$, $\tau_c = 8.4(1)$ min, and $c = 1.62(3) \times 10^{-4}$ min^{-1}.

f_c^{inf} and τ_c are of the same order of magnitude of the corresponding parameters f_b^{inf} and τ_b of the bead swelling factor $f_b(t)$, as it should be expected if both processes are linked to each other. In particular, it is remarkable that τ_b and τ_c become equal within their associated errors, while f_c^{inf}/f_b^{inf} 0.5, indicating that cluster swelling amplitude is smaller than that of bead itself. Besides, cluster swelling presents a secondary and slower step which becomes apparent in the $\kappa_n(t)$ behavior beyond about 37 min. At $t = 180$ min bead and clusters have swelled about 2.08 and 1.16 times, respectively. The initial volume fraction of particles in clusters must satisfy $0.073(6) \leq x_{pc0} \leq 1$, hence the non-interacting susceptibility of the particles must be in the range $5.8(2) \leq \chi \leq 79$ (these wide range of values will be considerable thinned later, at the light of other studies). Since the thermal equilibrium susceptibility of a non-interacting particle is $\chi = \frac{\mu_0\mu_p^2}{3V_pk_BT}$, where μ_0 is the vacuum susceptibility, μ_p the particle magnetic moment, k_B the Boltzmann constant and T the absolute temperature, this range of χ values corresponds to particle

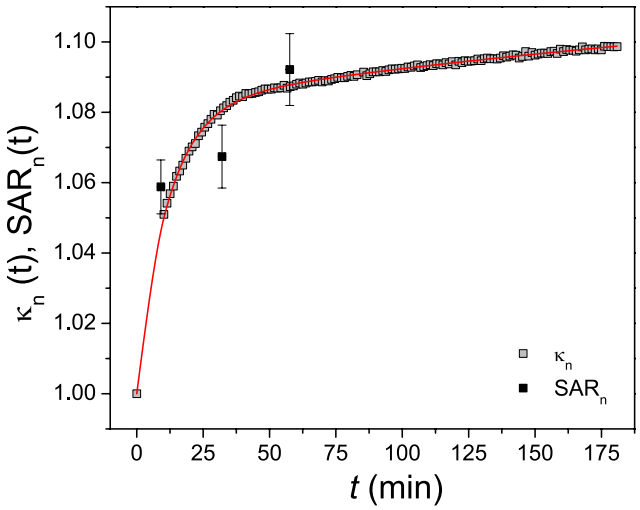

Fig. 5. Analysis of $\kappa_n(t)$ with the model of isotropic swelling of clusters described in the main text. Red line is the curve fitted with expressions (6) and (7). $SAR_n(t)$ results (black dots) are discussed below. (For interpretation of the references to colour in this figure legend, the reader is referred to the web version of this article.)

sizes between 5 nm and 17 nm, assuming they are made of an iron oxide with spontaneous magnetization of 51 emu/g (as it is concluded below, in paragraph following expression (13)) .

At times $t > 400$ min, the increase rate of κ diminishes (see Fig. 4b), and this magnitude decreases from about $t = 800$ min on. It was suspected that this unexpected behavior obeys to the additional oxidation of the iron oxide phases present in the particles, leading to some quantity of antiferromagnetic hematite. To verify this hypothesis two additional experiments were carried out. Section 3.3.2 presents the measurements of the magnetic moment of one dry bead as a function of applied field, before and after hydration for three days; and Section 3.3.3 presents a confocal Raman spectroscopy analysis of another dry virgin bead and of a bead which was hydrated during three days.

3.3.2. Magnetization cycles

A virgin bead was hydrated in 1 mL of milliQ water for three days and dried at room temperature.

Measurements of its magnetic moment μ vs. applied field H^A were performed in the dry state, before and after hydrating (see Fig. 6a). Moment at the highest field, 19000 Oe decreased from 0.0178 emu to 0.0160 emu, i.e. approximately 10%. In turns, low field dc susceptibility, obtained from the linear μ vs. H^A vs. region, decreased from 2.21×10^{-5} emu/Oe to 2.07×10^{-5} emu/Oe, i.e., nearly 6.3%. The diminution of both quantities as a result of three days hydration followed by drying is in agreement with the assumption that part of the magnetic material was transformed to a phase with lower specific moment.

3.3.3. Confocal Raman spectroscopy analysis

Confocal Raman spectroscopy was carried out on a virgin dry bead, and on a bead which was hydrated for 3 days. In Fig. 7 we show examples of Raman spectra taken at different bead regions before and after hydrating ((a) and (b, c), respectively). These spectra were recorded in a low power regime ($\leq$0.8 mW) to avoid laser-induced chemical-phase transitions, adding 10 accumulations with an exposure time of 10 s each.

The many spectra taken before hydrating showed evidences for magnetite and maghemite coexistence. The relative ratio between the bands indicates a greater abundance of magnetite (Fig. 7(a)). The spectra taken after hydration showed mostly presence of the same phases, though an increase of the relative maghemite abundance is determined from the bands ratio (Fig. 7(b)). Besides, after hydration, one tenth of the spectra showed hematite bands (Fig. 7(c)), which has a high Raman activity even at very low concentrations [11,12].

Considering that susceptibilities of magnetite and maghemite are alike at RT, being in fact that of maghemite slightly higher ([13], see Fig. 5, top panel) the diminution experienced by κ from 800 min onwards is essentially ascribed to the formation of hematite. An approximate estimation of the relative fraction F of magnetite/maghemite transformed into hematite can be made by $F = \Delta\kappa/\kappa_{max}$, where $\Delta\kappa$ is the ac susceptibility reduction from its maximum value in Fig. 4b to its final value (gray bar in the same figure), or the dc susceptibility reduction after hydration in Fig. 6b. This estimation gives $F =$ 0.07 in both cases, in general agreement with what was observed by Raman spectroscopy. Another estimation could be made from the reduction of the magnetic moment registered at the highest applied field of 19000 Oe after three days of hydration. This reduction amounts to about 10%, nevertheless it must be considered that it may not be only the result of hematite formation, since maghemite has also a specific moment lower than magnetite. Hence percent transformation into hematite should be between 7% and 10%.

4. SAR studies

Experiments of Specific Absorption Rate (SAR) of power dissipated by the particles in response to the application of a RF field, were performed in two ways. The first one was a concept experiment in which a single dry bead was located at the center of the RF duty coil (Fig. 8(a,b)) and temperature variations were recorded with an infrared camera while RF field was kept on. In the second experiment 4 beads with a

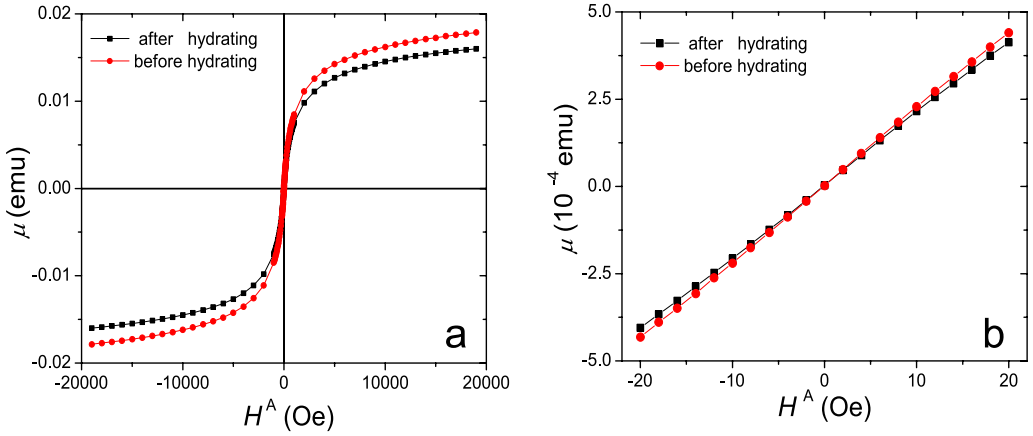

Fig. 6. a) curves of magnetic moment of a dry bead obtained before and after hydration for three days. b) central parts of curves shown in a).

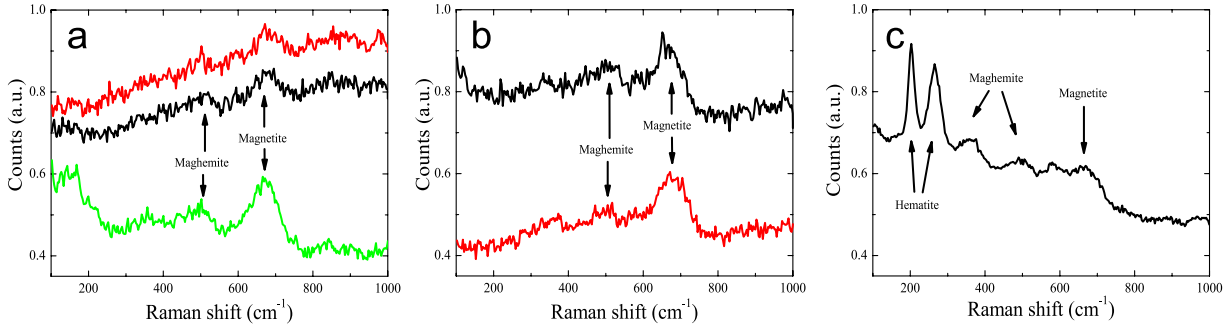

Fig. 7. Raman spectra of one bead before hydrating (a) and after 3 days hydration (b, c). Spectra in (a, b) show magnetite and maghemite bands, spectra in (c) shows also hematite bands.

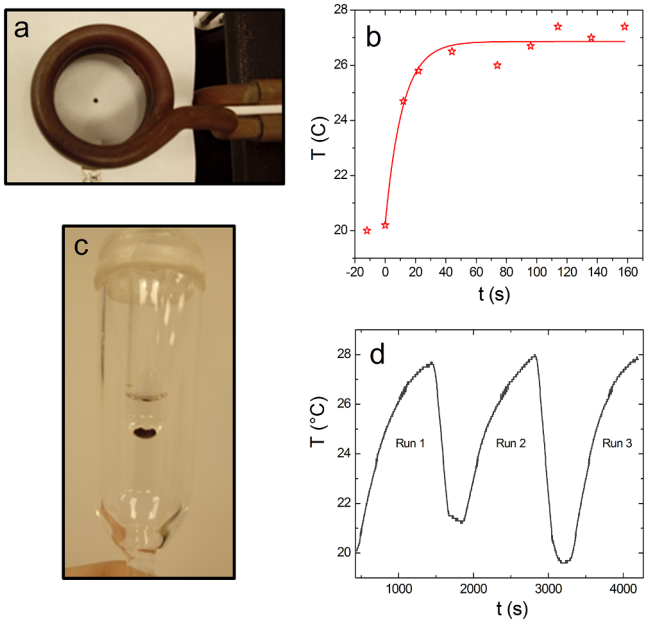

Fig. 8. (a) Bead located near the center of the RF duty coil (25 mm inner diameter). (b) temperature of the bead as a function of time during 160 s, recorded with an infrared camera (amplitude of 700 Oe and frequency of 260 kHz). (c) Four beads in 300 μL of milliQ water placed inside the calorimeter clear Dewar bottle (it fits into the coil shown in (a)). (d) Temperature of water vs. time for the three runs with RF field on (growing portions of the experimental curve) and off.

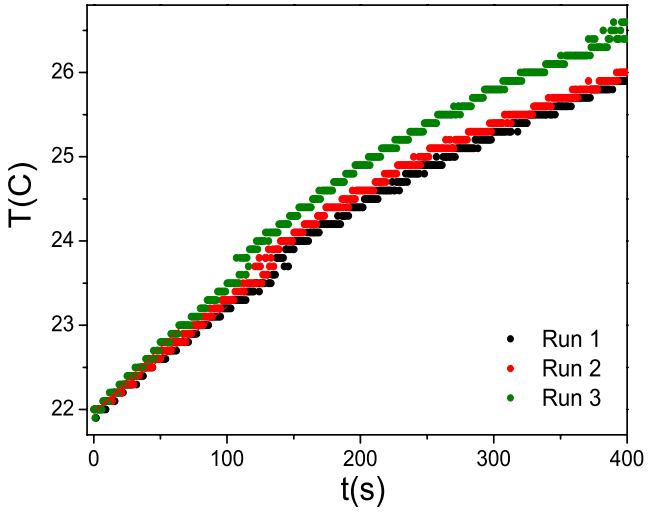

Fig. 9. Redraw of runs 1, 2 and 3 of Fig. 8(d). Time $t = 0$ s was reset at the instants at which RF field was set on.

total mass of 4.8(1) mg were immersed in 300 μL of milliQ water held inside a small transparent Dewar bottle, located at the center of the RF duty coil. Temperature variations were registered using semiconductor, temperature to light transducers, attached to a thin light-guide and connected to a signal processor. Temperature recordings were obtained as a function of time during about 17–20 min, while the beads underwent hydration (Fig. 8(c, d)) under RF irradiation, and continued 7–10 min more with the RF field off in order to allow cooling down to RT. After attaining RT, the experiment was repeated (twice) while beads continued hydrating. The value of the slope $\Delta T/\Delta t$ for each repetition was determined over a period of no more than 1 min, to minimize the effects of swelling during measurement. SAR was calculated as [14]

$$SAR = \frac{C}{[c]}\frac{\Delta T}{\Delta t} \tag{9}$$

where C is the specific heat of the volume being heated (essentially water), and $[c]$ is the mass fraction of particles in that volume. The experiment performed on the dry bead demonstrated that dissipation was enough to increase the bead temperature more that 4 K, even when losses to the environment were large, and prevented a reliable determination of SAR.

For the 4 beads immersed into water, slope $\left.\frac{dT}{dt}\right]_{T_{lab}}$ was obtained by fitting of the $T(t)$ data contained within a small temperature interval centered at $T = T_{lab}$, with a linear function of time [14]. In Fig. 9 we have redrawn Fig. 8(d) data, after redefining the origin of time for each of the three runs. Fitting was performed within the time region between 5 and 65 s. Values of $\left.\frac{dT}{dt}\right]_{T_{lab}}$ of 0.01250(2), 0.01335(2) and 0.01555(2) K/s, were obtained for runs 1, 2, 3 respectively. The relative mass fraction of particles in the heated volume can be expressed as $[c] = \frac{m_p}{m_b + m_w}$, where $m_b = 4.8(1) \times 10^3$ g is the mass of the 4 beads, $m_w = 0.300(3)$ g is the mass of water, and m_p is the mass of particles in the 4 beads. Dividing numerator and denominator of this expression by m_b, it becomes $[c] = \frac{x^m_{pb}}{1 + m_w/m_b} = 0.0041(2)$, where $x^m_{pb} = 0.26(1)$ is the mass fraction of particles in the beads. Using $C = 4.186$ J/Kg, we obtain values of $SAR = 12.8(6), 13.6(7), 15.9(8)$ W/g$_p$ for runs 1, 2, 3, respectively. These $SAR(t)$ results, correspond to hydration times of 9, 32, and 58 min, respectively, and indicate that SAR is an increasing function of the apparent susceptibility κ (see Fig. 5). This result should be analyzed at the light of the prediction of the linear response model [14,15],

$$SAR \propto \frac{\pi\mu_0 H_0^{A2} f\kappa}{\rho}\frac{2\pi f\tau_R}{1 + (2\pi f\tau_R)^2} \tag{10}$$

where $f = 260$ kHz is the RF field frequency, $H_0^A = 700$ Oe is the RF field amplitude, ρ the particles' density and τ_R the relaxation time of the particle magnetic moment. Indeed, within the frame of this model, SAR and κ are proportional to each other, although part of the

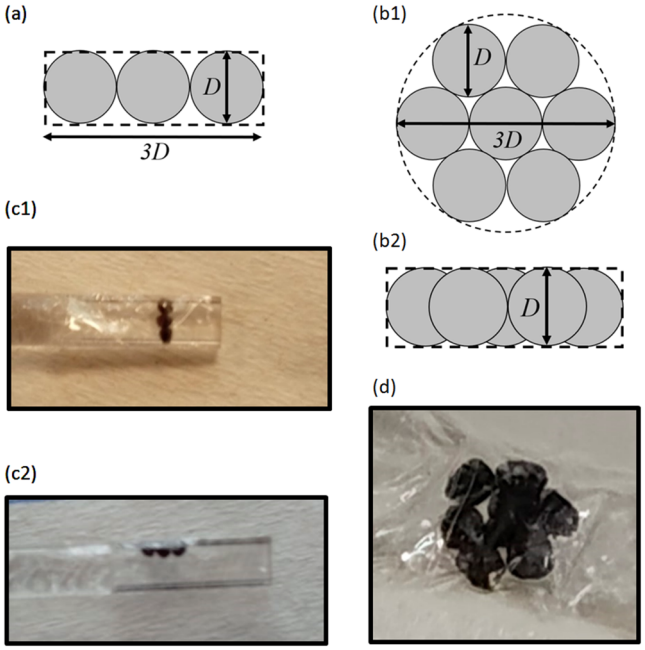

Fig. 10. Arrays of dry beads. (a) Scheme of the chain-like array. Top (b1) and side (b2) views of the scheme of the disk-like array. Actual chain-like array oriented in direction perpendicular (c1) and parallel (c2) to the magnetic field of VSM. (d) Actual disk-like array.

proportionality factor, the frequency factor $\frac{2\pi f\tau_R}{1+(2\pi f\tau_R)^2}$, depends on the relaxation time which is strongly affected by the intensity of the dipolar interactions [16,17]. *SAR* values have been custom-normalized in order to allow a comparison with susceptibility ones (Fig. 5). It would be desirable to record $SAR(t)$ instantaneously, as a function of hydrating time, in order to make a continuous comparison of its evolution with that of $\kappa(t)$, starting at $t = 0$ s. ESAR technique, recently implemented [18] would be an appropriate methodology to this end.

5. Experiments on superstructures (arrays of dry beads)

To learn on the effect of inter-bead interactions (shape of the superstructure), experiments were performed on a single bead and on two different arrays of them: a chain-like array composed of three beads in a row, and a disk-like one composed of seven beads closely packed onto a plane (see Fig. 10). These arrays were chosen because they can be associated to high aspect regular bodies, like cylinder and disk, which possess non-neglectable magnetic anisotropy. Beads were measured individually and forming the two arrays, along their longest and shorter dimensions. The arrays constitute samples with a higher degree of complexity and consequently need to be described by more complex effective demagnetizing tensors. Now we must consider particles, clusters and superstructures, hence we propose that, the tensor component in one principal direction is given by

$$N^E = N^c x_{pc}(1 - x_{cb}) + N^b x_{pc} x_{cb}(1 - x_{bs}) + N^s x_{pc} x_{cb} x_{bs}, \tag{11}$$

where $N^c = N^b = 1/3$, while N^s can be obtained from the literature for specimens with cylinder and disk shapes. On the other hand, x_{bs}, the volume fraction of beads in the specimen, can be obtained from geometric considerations. For the chain, $x_{bs} = 2/3$ and for the disk $x_{bs} = 14/27$. The chain has an aspect ratio $\gamma = L/D = 3$, so the principal components of the specimen demagnetizing tensor are [19] $N^{s\parallel} = 0.128$, and $N^{s\perp} = 0.436$, for the parallel (axial) and perpendicular directions, respectively. The disk is a short cylinder which has an aspect ratio $\gamma = L/D = 1/3$, and demagnetizing tensor principal components [19] $N^{s\parallel} = 0.573$, and $N^{s\perp} = 0.214$. From the discussion in this paragraph, (11) can be written for both arrays as

Table 1
Specimens (superstructures), experimental configurations, effective demagnetizing factors, normalized measured dc susceptibilities, and last term values of Eq. (12), which are the abscissa values in Fig. 12.

Specimen	Configuration	N^E	κ_i^n	$x_{bs}(N^s - 1/3)$
Single bead		$\frac{x_{pc}}{3}$	1	0
Chain	Parallel	$\frac{x_{pc}}{3} - 0.010$	1.04(1)	−0.137(1)
Chain	Perpendicular	$\frac{x_{pc}}{3} + 0.005$	0.97(1)	0.068(2)
Disk	Parallel	$\frac{x_{pc}}{3} + 0.009$	0.98(1)	0.124(6)
Disk	Perpendicular	$\frac{x_{pc}}{3} - 0.005$	1.06(1)	−0.062(4)

$$N^E = \frac{x_{pc}}{3} + x_{ps}\left(N^s - \frac{1}{3}\right), \tag{12}$$

where $x_{ps} = x_{pc}x_{cb}x_{bs}$. Notice that if were $N^s = 1/3$, then $N^E = x_{pc}/3$, in coincidence with the value of N^E for a single bead (and the one given by (5) for $t = 0$). This obeys to a general property of the effective demagnetizing tensor. When it is referred to the magnetization of the particles' phase, if all tensor components in a principal direction are equal ($N^s = N^b = N^c = N$), then $N^E = x_{pc}N$. Notice also that expression (12) is independent of x_{bs}. Since x_{ps} and N^s are known (x_{ps} and N^s have different values for each array, and N^s has also a different value for each experiment orientation) the only unknown in (12) is x_{pc}. Indeed, as $x_{ps} = 0.073x_{bs}$, for the chain-like array we have $x_{ps} = 0.049(9)$, and for the disk array, $x_{ps} = 0.038(7)$. In Table 1 we list the expressions of N^E for the measured specimens and orientations. The magnetization M of each of the three beads used to build up the chain-like array was measured as a function of H^A at room temperature (Fig. 11(a)). The curves are typical of polydisperse distributions of mostly superparamagnetic particles. They present small coercivities of the order of H_c= 400 A/m (5 Oe), which indicates that a small fraction of particle magnetic moments μ are blocked at RT. We use this coercivity to make an estimation of the fraction of particle moments blocked at RT in order to justify the analysis of the M vs. H curves with Langevin-like functions. Such fraction can be estimated by the quotient H_c/H_K where H_K is the anisotropy field, $H_K = 2K_{eff}/(\mu_0 M_S)$. We will assume, based on the Raman results, that the oxide is a mixture of magnetite and maghemite with a magnetite percentage between 60 and 80%. Furthermore, in small particles, the effective anisotropy is larger than the bulk one, because of the contributions from surface and shape, in most cases, by a factor between 1.3 and 1.84 [20]. By considering the range of magnetite percentages p in the oxide, and the ranges of anisotropy values, both for magnetite and maghemite particles the range of possible anisotropy fields can be calculated as

$$H_K = 2(p\ K_{eff}^{magn} + (1-p)\ K_{eff}^{magh})/(\mu_0\ p\ M_S^{magn} + \mu_0\ (1-p)\ M_S^{magh}),$$

where K_{eff}^{magn} and K_{eff}^{magh} are the effective anisotropies of magnetite and maghemite, respectively.

The result is that the anisotropy field can take values in the range 4.8×10^4 A/m $\leq H_K \leq 7.6 \times 10^4$ A/m. The upper value of H_K rises up to 1.31×10^5 A/m if we use the experimental value of the saturation magnetization $M_S = 51$ emu/g. From this, the fraction of particles which are blocked at RT can be estimated as $0.003 \leq H_c/H_K \leq 0.008$. We have used magnetite and maghemite bulk properties $M_S^{magn} = 92$ emu/g, $M_S^{magh} = 76$ emu/g, $K^{magn} = 13 \times 10^3$ J/m^3 and $K^{magh} = 5 \times 10^3$ J/m^3 from [13]. This estimation supports the use of Langevin-like functions to analyze the M vs. H^A cycles.

For the seven beads employed to set up the disk-like array M vs. H^A cycles are very similar to those shown in Fig. 11(a) and (b) with just slight differences in their slopes at low fields. The M vs. H^A curves were analyzed assuming a LogNormal distribution $l^E(\mu^E)$ of moments ($P(\mu)$) whose director cosines along H^A orientation follow Langevin functions $L(y)$, with $y = \mu_0\mu(H^A \pm H_C)/k_BT$, i.e., allowing for a small coercive

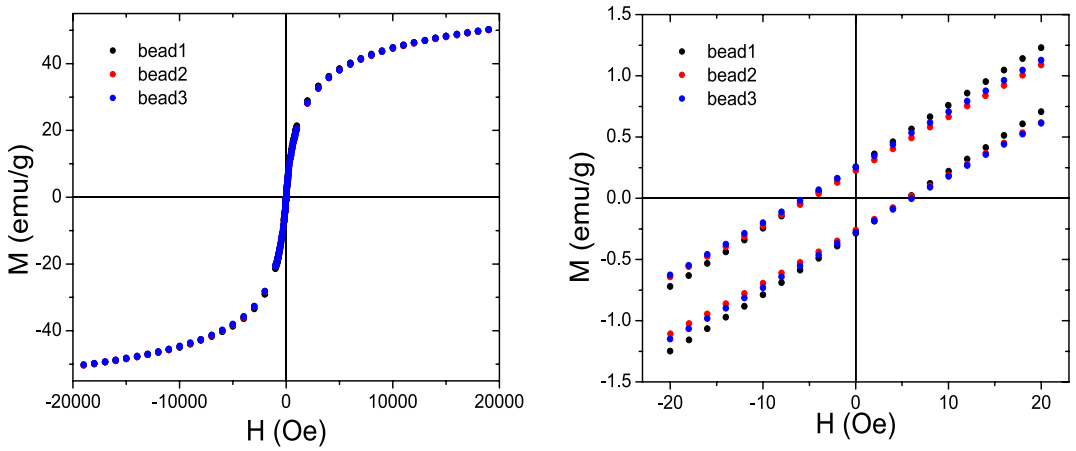

Fig. 11. Isothermal magnetization cycles of individual beads used for the chain-like array. (a) Full curves displaying mostly superparamagnetic behavior. (b) Detail illustrating the low-field, linear-regime region used to calculate the apparent susceptibility κ.

field H_C. It has been pointed out that this model is only approximated for a random distribution of superparamagnetic particles having their easy axes randomly orientated in fixed directions [21]. However, it gives a very good description of the low field susceptibility, being the approximation at other field values acceptable when the anisotropy contribution KV_p is small in comparison with the Zeeman interaction $\mu_0\mu H$, where K is the effective anisotropy density and V_p the particle volume. Assuming, from the aspect of the experimental curves, that the anisotropy energy does not modify substantially the Langevin-like response of the magnetic moments, fitting of the cycles was done with the function [22]

$$M(H^A, T) = \frac{1}{\langle V_p^E \rangle} \int \mu_p^E L\left(\frac{\mu_0 \mu_p^E (H^A \pm H_C)}{k_B T}\right) l^E(\mu_p^E) d\mu_p^E + M_0 + \chi_o H^A \tag{13}$$

where $\langle V_p^E \rangle$ is the mean effective volume and μ^E the effective moment of the particles, $l^E(\mu_p^E)d\mu_p^E$ is the LogNormal distribution of effective moments, M_0 stands for an offset constant, and χ_o takes into account potential paramagnetic or diamagnetic contributions from PVA and sample holder. By effective, or apparent, moments and volumes, we refer to the values of these quantities retrieved by the analysis of magnetic measurements performed on a specimen where the interactions among particles could not be neglected, when the analysis is performed in terms of the applied field H^A and not in terms of the effective field acting on the particles, $H^E = H^A + H^D$. The fitting of M vs. H^A curves leads to the following results: $\sigma = 1.413(2)$, $\langle \mu_p^E \rangle = 1494(9)\mu_B$, where μ_B is the Bohr magneton, coercive field $H_C = 5.48(1)$ Oeor 436(1) A/m, and saturation magnetization $M_s =$ 51 emu/g. Assuming that particles are spherical, made essentially of magnetite, with an average moment projection (in the applied field direction) per Fe ion $\mu_{Fe} =$ $0.7\mu_B$ at RT (consistent with the saturation magnetization), cubic cell parameter $a = 0.839$ nm and 24 Fe ions per cell [23,24], a mean volume $\langle V_p^E \rangle = 53.0(2)$ nm^3 and an associate diameter $D_p^E = 4.70(1)$ nm are obtained. It has been shown that the powers μ_p^n of the moment of a non-interacting particle are related to the powers of the effective moments $(\mu_p^E)^n$ by $\mu_p^n = \frac{\chi}{\kappa}(\mu_p^E)^n$ [7]. This relationship applies also to mean values, and, since saturation magnetization should not be affected by dipolar interactions, it applies also to the particles' volume $\langle V_p \rangle = \frac{\chi}{\kappa}\langle V_p^E \rangle$. Hence, μ_p, V_p, and D_p are always larger than μ_p^E, V_p^E, and D_p^E, as well as their powers and mean values, respectively. For the case just analyzed, assuming $K = 2 \times 10^4$ J/m^3 [13], $\mu_0\mu H^A = K\langle V_p^E \rangle$ for $H^A = 815$ Oe $= 6.486 \times 10^4$ A/m, rendering reasonable the analysis with the model employed.

In order to compare the susceptibilities obtained from the several measured cycles: single beads, chain and disk-like arrays, in the two principal orientations for the arrays, the following procedure was followed: (a) all measurements were performed under same experimental conditions, (b) susceptibilities of the chain, and disk-like, arrays in the parallel and perpendicular orientations were normalized by the corresponding average susceptibility of the three, or seven, beads forming the arrays as

$$\kappa_{\parallel,\perp}^n = \frac{\Delta\mu_{\parallel,\perp}/\Delta H^A}{\sum \Delta\mu^{bi}/\Delta H^A},$$

where $\mu_{\parallel,\perp}$ is the moment of the array, and μ^{bi} is the moment of bead i. The variations are taken within the same ΔH^A interval of approximately 3.18x10^3 A/m (approximately 40 Oe). Then the value of $\Delta\mu_{\parallel,\perp}/\Delta H^A$ was obtained for each specimen by fitting the experimental data with a linear function. The normalization procedure was done to avoid, as much as possible, uncertainties originated in compositional differences between the beads used in both arrays. Obviously, this normalization led to $\kappa^n = 1$ for a single bead. Values of κ^n for all configurations are given in the fourth column of Table 1. Fig. 12 is a representation of κ^n as a function of the magnitude listed in the last column of Table 1, $x_{ps}\left(N^s - \frac{1}{3}\right)$. The red line is a fit with the expression

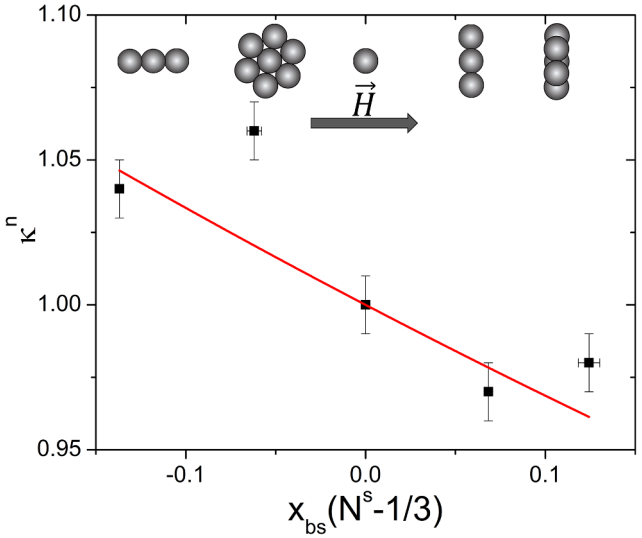

Fig. 12. Dots: representation of the normalized apparent susceptibility κ^n as a function of $x_{bs}(N^s - 1/3)$ for the two superstructures measured in the two perpendicular principal directions indicated in the figure, and for a single bead (Table 1). Direction of the applied field relative to the superstructures is indicated in the upper part. Redline: best fit with expression (14).

$$\kappa_i^n = \frac{1 + x_{pc}\chi/3}{1 + \left(\frac{x_{pc}}{3} + x_{psi}\left(N_i^s - \frac{1}{3}\right)\right)\chi} = \frac{1 + y_{pc}/3}{1 + y_{pc}(1/3 + x_{cb}x_{bsi}(N_i^s - 1/3))}, \quad (14)$$

where κ_i^n, $y_{pc} = x_{pc}\chi$ (as before), and x_{psi}, N_i^s refer to the configurations listed in Table 1. Parameter y_{pc} was kept fixed at the value retrieved from the fitting of $\kappa_n(t)$, $y_{pc} = 5.8(2)$. The value of x_{cb} retrieved from the fit with expression (14) is $x_{cb} = 0.16(5)$, which indicates that about 16% of the bead volume is occupied by the particles' clusters. Using $x_{pb} = 0.073(6)$ we obtain $x_{pc} = 0.46(15)$. On the other hand, $\chi = y_{pc}/x_{pc} = 13(4)$.

Using the relationship $\langle V_p \rangle = \frac{\chi}{\kappa}\langle V_p^E \rangle$ with this value of χ, and values of $\kappa = 2.6(2)$ (derived from the red-star data in Fig. 4b) and $\langle V_p^E \rangle = 53.0(2)$ nm^3, we can estimate the actual particle volume as $\langle V_p \rangle = 260(80)$ nm^3, with an associated diameter $D_p = 8(1)$ nm.

6. Summary and conclusions

We have synthesized PVA/iron oxide milli-size beads by means of a one-pot route. Beads have high mass fraction of iron oxide particles $x_{pb}^m = 0.26(1)$, present a saturation magnetization of 51 emu per gram of particles, and swell 208% by hydration in milliQ water. Dependency of the volume of a bead on time of hydration is well described by Eq. (5), with a swelling saturation parameter $f_b^{inf} = 2.077(1)$ and a time constant $\tau_b = 8.4(1)$ min. The evolution of the ac susceptibility as a function of hydration time closely reflects the bead swelling behavior. The measured susceptibility $\kappa_n(t)$ was analyzed in terms of the susceptibility χ of a non-interacting particle and the effective demagnetizing factor N^E of the bead (Eq.(6)), dependent in turns on the clusters swelling function (8). Best fitted parameters were the swelling parameter $f_c^{inf} = 1.130(1)$, the time constant $\tau_c = 8.4(1)$ min, the linear swelling constant $c = 1.62(3) \times 10^{-4}$ min^{-1}, and the susceptibility parameter $y_{pc} = 5.8(2)$. It was found that time constants τ_b, τ_c of beads and clusters swelling are the same within experimental error, while clusters swell only up to 16% in comparison to 208% of beads. The increase of $\kappa_n(t)$ at times beyond ~40 min was explained by an additional swelling mechanism for the clusters, represented by the linear term in (8). The decrease of $\kappa_n(t)$ for $t \geq 580$ min was explained by the occurrence of a gradual oxidation of magnetite / maghemite to hematite in water environment. This decrease of the ac susceptibility is consistent with the diminution of the dc susceptibility and high field magnetization observed in the M vs. H cycles of a bead hydrated for three days and dried, in comparison to the values obtained from the same bead before hydration. Formation of hematite was confirmed by Raman experiments. It was concluded that about 7 to 10% of the original oxides were converted into hematite.

Recorded *SAR* values were moderate, between 13 and 16 W/g$_p$ (referred to particles' mass) but potentially adequate, for example, for RF triggered drug release applications, especially considering that the high mass fraction of particles in the beads, $x_{pb}^m = 0.26(1)$, provides a strong potential for electromagnetic energy transduction into heat. *SAR* was recorded calorimetrically in water, while particles were still hydrating. The recorded values, 12.8(6), 13.6(7), 15.9(8) W/g$_p$, were measured at hydration times of 9, 32, and 58 min, respectively. These increasing results are consistent with ac susceptibility being a growing function of swelling.

Experiments with the two arrays of beads in two perpendicular principal directions were consistently described with the mean field model (MFISP) for the effect of interparticle dipolar interactions [7], by considering two hierarchies of clustering: beads, and clusters within the beads, and assuming a value 1/3 for the demagnetizing factors associated with average beads and clusters shapes in any direction.

From the whole set of experiments, it was possible to estimate values for the volume fractions of particles in clusters and clusters in beads, given by $x_{pc} = 0.46(15)$ and $x_{cb} = 0.16(5)$, i.e. almost half of clusters volume would be filled with particles, providing a quite strong dipole–dipole interaction. It was also possible to estimate the susceptibility of non-interacting particles $\chi = 13(4)$, five times larger than the measured, or apparent, one. The magnetic estimation of the particles mean diameter, after getting rid of dipolar effects, was $D_p = 8(1)$ nm.

The MFISP model [7] for the effects of dipole–dipole interactions in magnetic particles' systems, proved to be a convenient and efficient tool for the analysis of magnetization studies of complex 3d dispersions of magnetic particles, allowing an experimental determination of relevant physical quantities, otherwise not accessible by magnetic measurements.

Declaration of Competing Interest

The authors declare that they have no known competing financial interests or personal relationships that could have appeared to influence the work reported in this paper.

Acknowledgements

LMS and VAA acknowledge the financial support of CONICET, ANPCyT and UNMdP, and DGA, GAMM, DMA, PMZ and FHS the financial support of CONICET, ANPCyT and UNLP. This study was partially supported by CONICET Grant No. PIP11220110100720CO, ANPCyT Grant No. PICT-2017-1748 and UNLP Grant No. 11/X807, from Argentina, as well as the TWAS-CONICET Associateship Scheme Grant, Ref. 3240302357 (AAVT).

References

[1] Paolo Allia, Paola Tiberto, J. Nanopart. Res. 13 (12) (2011) 7277.
[2] B. Hillebrands, C. Mathieu, D. So, S. Riedling, O. Büttner, A. Frank, C. Chappert, J. Magn. Soc. Jpn 23 (1) (1999) 670.
[3] Rudolf Weeber, Melissa Hermes, Annette M Schmidt, Christian Holm, J. Phys.: Condens. Matter 30 (2018) 063002.
[4] Ting-Yu Liu, Hu. Shang-Hsiu, Tse-Ying Liu, Dean-Mo Liu, San-Yuan Chen, Langmuir 22 (2006) 5974.
[5] L.M. Sanchez, D.G. Actis, J.S. Gonzalez, P. Mendoza Zélis, V.A. Alvarez, J. Nanopart. Res. 21 (3) (2019) 64.
[6] Li He Zhou, Benzhao Zhang, Faai, ACS Appl. Mater. Interfaces 4 (2012) 192.
[7] F.H. Sánchez, P. Mendoza Zélis, M.L. Arciniegas, M.B.G.A. Pasquevich, F. van Raap, Phys. Rev. B 95 (2017) 134421.
[8] P. Mendoza Zélis, V. Vega, V.M. Prida, L.C. Costa-Arzuza, F. Béron, K.R. Pirota, R. López-Ruiz, F.H. Sánchez, Phys. Rev. B 96 (2017) 174427.
[9] E. Goiti, M.M. Salinas, G. Arias, D. Puglia, J.M. Kenny, C. Mijangos, Polym. Degrad Polym. Degrad. Stab. 92 (12) (2007) 2198.
[10] B. D. Cullity, Introduction to Magnetic Materials, Hoboken, NJ: (IEEE/Wiley, 2009.
[11] I. Chourpa, L. Douziech-Eyrolles, L. Ngaboni-Okassa, J.-F. Fouquenet, S. Cohen-Jonathan, M. Souce, H. Marchais, P. Dubois, Analyst 130 (2005) 1395.
[12] Jesica M. J. Santillan, David Muñeton Arboleda, Diego F. Coral, Marcela B. Fernandez van Raap, Diego Muraca, Daniel C. Schinca, and Lucia B. Scaffardi, Chemphyschem, vol. 18, pp. 1, 2017.
[13] Jeppe Fock, Lara K. Bogart, David González-Alonso, Jose I Espeso, Mikkel F. Hansen, Miriam Varón, Cathrine Frandsen, Quentin A. Pankhurst, J. Phys. D: Appl. Phys. 50 (2017) 265005.
[14] M. Elisa de Sousa, B. Marcela, Fernandez van Raap, Patricia C. Rivas, Pedro Mendoza Zelis, Pablo Girardin, Gustavo A. Pasquevich, Jose L. Alessandrini, Diego Muraca, Francisco H. Sanchez, J. Phys. Chem. C 117 (2013) 5436.
[15] R.E. Rosensweig, J. Magn. Magn. Mater. 252 (2002) 370.
[16] J. L. Dormann, D. Fiorani, and E. Tronc, pp. 283, New York: edited by I. Prigogine and S. A. Rice (Wiley), 1997.
[17] G.T. Landi, J. Appl. Phys. 113 (2013) 163908.
[18] J. Bruvera, D.G. Actis, M.P. Calatayud, P. Mendoza Zélis, J. Magn. Magn. Mater. 491 (2019) 165563.
[19] Du-Xing Chen, James A. Brug, Ronald B. Goldfarb, IEEE Trans. Magn. 27 (4) (1991) 3601–3619.
[20] D. Fiorani, A.M. Testa, F. Lucari, F. D'Orazio, H. Romero, Phys. B 320 (2002) 122.
[21] J. Carrey, B. Mehdaoui, M. Respaud, J. Appl. Phys. 109 (2011) 083921.
[22] P. Mendoza Zélis, D. Muraca, J.S. González, G.A. Pasquevich, V.A. Álvarez, K.R. Pirota, F.H. Sánchez, J Nanopart Res 15 (2013) 1613.
[23] https://www.mindat.org/min-2538.html.
[24] Amedea B. Seabra, Milena T. Pelegrino and Paula S. Haddad, in Nanostructures for Antimicrobial Therapy (Nanostructures in Therapeutic Medicine Series), Ed. By Anton Ficai and Alexandru Mihai Grumezescu, Elsevier, 2017.